Dissipation in Quantum Systems

Shangrun Lu[*] and Binyang Jian[†]

1 Sun Yat-sen University, School of Physics, Guangzhou 510275

(Dated: June 14, 2024)

Quantum information processing relies on the precise control of non-classical states in the presence of numerous uncontrolled environmental degrees of freedom. The interaction between these relevant degrees of freedom and the environment is typically seen as detrimental because it leads to energy dissipation and quantum state decoherence. However, when dissipation is precisely controlled, it can become a crucial tool for manipulating quantum information. Dissipative engineering can achieve quantum measurement, quantum state preparation, and quantum state stabilization. This paper systematically introduces quantum dissipation and its applications in quantum error correction and quantum simulation.

Keywords: Lindblad master equation, Quantum dissipation, Quantum simulation, Quantum error correction

I. INTRODUCTION

Dissipation often exists in arbitrary quantum systems. Uncontrolled dissipation could destroy coherence, degrade the fidelity of quantum gates in quantum information as well as add noise to measurement signals. All attempts to build quantum computers are hindered by noise generated by uncontrolled interactions between qubits and their environment. However, carefully tuned quantum noise in the form of engineered dissipation can be harnessed for various purposes, such as protecting states from unwanted noise, controlling the dynamical evolution of systems, and implementing constraints.

The theory of dissipation is generally described in the form of master equation and quantum operations. The former emphasizes dissipation, while the latter is more generalized. We mainly use the form of master equation in this paper to elaborate quantum dissipation and introduce some of its applications.

II. LINDBLAD MASTER EQUATION

A. Mathematical Expressions

The evolution of the density matrix of a closed system satisfies the Liouville equation. However, general closed systems tend to be large, and we often focus on a small subsystem. Assuming the combined Hamiltonian of the quantum subsystem and the external environment is

$$\hat{H}_{all} = \hat{H}_S \otimes \hat{I}_B + \hat{I}_S \otimes \hat{H}_B + \lambda\hat{H}_{SB}, \quad (1)$$

where $\hat{H}_S$ and $\hat{H}_B$ represent the free Hamiltonians of the quantum system and the environment, respectively, $\hat{H}_{SB}$ denotes the coupling between the two systems, and λ is the coupling coefficient which is generally considered to be a small quantity relative to the energy scale of the system.

In the Schrödinger picture, the dynamical evolution of the system is given by the Liouville equation:

$$\frac{d\rho(t)}{dt} = \frac{1}{i\hbar}\left[\hat{H}_{all}, \rho\left(t\right)\right]. \quad (2)$$

Using the Born approximation, Markov approximation, and rotating wave approximation, the evolution of the reduced density matrix of the subsystem satisfies the Lindblad master equation[1–3]:

$$\begin{aligned}\frac{d\rho_s(t)}{dt} =& \frac{1}{i\hbar}\left[\hat{H}, \rho_s\left(t\right)\right] \\ &+ \sum_k \gamma_k\left[\hat{L}_k\rho_s\hat{L}_k^\dagger - \frac{1}{2}\left\{\hat{L}_k^\dagger\hat{L}_k, \rho_s(t)\right\}\right].\end{aligned} \quad (3)$$

Where $\hat{H} = \hat{H}_S + \hat{H}_{LS}$ represents the Hamiltonian of the subsystem plus the correction term induced by the environment, corresponding to the Lamb shift term in quantum electrodynamics (QED), which is generally small and can be neglected. $\gamma_k \geq 0$ is the dissipation rate, characterizing the strength of dissipation, and L_k is the Lindblad operator, which represents the operator that causes the system state to change due to the coupling between the system and the environment.

B. Quantum Jump Theory.

Quantum jump theory (quantum trajectory theory) is a more intuitive way of deriving the master equation than the Born Markov approximation.

Considering the dissipation of a cavity field in quantum optics[4], for photons in a single-mode cavity, they can be absorbed by the cavity walls. Assuming that the cavity walls are at absolute zero temperature (T=0).

Assuming that the cavity field before a jump occurs is in the state $|\psi\rangle$, the probability δ P of a photon being absorbed within a time interval δ t should be proportional to the time interval and the average photon

———

[*] lushr3@mail2.sysu.edu.cn

[†] jianby3@mail2.sysu.edu.cn

number $\langle\psi|a^{\dagger}|\psi\rangle$ in the state $|\psi\rangle$, so that

$$\delta P = \gamma\langle\psi|a^{\dagger}|\psi\rangle\delta t, \qquad (4)$$

where γ is the photon loss rate.

The normalized quantum state after a photon jump is

$$|\psi\rangle \rightarrow |\psi_{jump}\rangle = \frac{a|\psi\rangle}{[\langle\psi|a^{\dagger}|\psi\rangle]^{1/2}} = \sqrt{\frac{\gamma\delta t}{\delta P}}a|\psi\rangle. \qquad (5)$$

The probability of a photon not being absorbed within the time δt is $(1-\delta P)$. Assume the effective Hamiltonian for the non-unitary evolution of the cavity field is $H_{eff} = H - i\frac{\gamma}{2}a^{\dagger}a$. When a photon is not absorbed, the cavity field evolves to

$$|\psi\rangle \rightarrow |\psi_{no-jump}\rangle = \frac{e^{-iH_{eff}\delta t}|\psi\rangle}{\left[\left\langle\psi\left|e^{iH_{eff}^{\dagger}\delta t}e^{-iH_{eff}\delta t}\right|\psi\right\rangle\right]^{1/2}}$$
$$\approx \frac{[1 - iH\delta t - a^{\dagger}a(\gamma/2)\delta t]|\psi\rangle}{(1-\delta P)^{1/2}}. \qquad (6)$$

Therefore

$$\rho(t+\delta t) = \rho(t) - i\delta t[H,\rho(t)]$$
$$+ \frac{\gamma}{2}\delta t\left\{2a\rho(t)a^{\dagger} - a^{\dagger}a\rho(t) - \rho(t)a^{\dagger}a\right\}. \qquad (7)$$

When $\delta t \rightarrow 0$,

$$\frac{d\rho}{dt} = -i[H,\rho] + \frac{\gamma}{2}\left\{2a\rho(t)a^{\dagger} - a^{\dagger}a\rho(t) - \rho(t)a^{\dagger}a\right\}. \qquad (8)$$

This is known as the quantum master equation, which describes the time evolution of the optical field in a single-mode cavity under the condition of loss at absolute zero temperature. It is essentially the dissipation equation for the cavity field, and it is consistent with the results given by the Lindblad master equation, where the Lindblad operator in this case is a. Meanwhile, the above equation can be expressed as

$$\frac{d\rho}{dt} = -i(H_{eff}\rho - \rho H_{eff}^{\dagger}) + \gamma a\rho(t)a^{\dagger}, \qquad (9)$$

$H_{eff} = H - i\frac{\gamma}{2}a^{\dagger}a$, which describes the evolution governed by a non-Hermitian effective Hamiltonian, along with the quantum jumps induced by the coupling with the environment.

In the following, dissipation will be employed to feedback the measurement and control the dynamic evolution of the system. We first introduce the quantum Zeno effect.

III. ZENO EFFECT

A. What is Zeno Effect

According to Zeno's paradox, when Achilles reached the starting point of the turtle, the turtle had moved
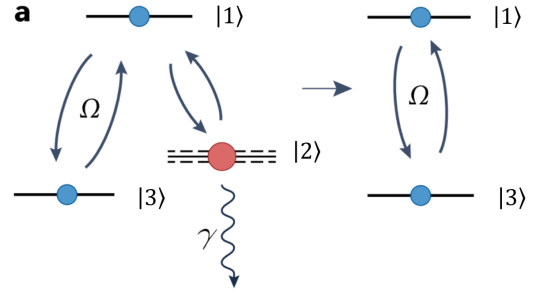

FIG. 1. Collapse of a three-level energy system into a two-level subspace. Figure reproduced from [5].

forward for a certain distance, and this process repeated indefinitely, rendering Achilles unable to catch up with the turtle. For an arrow in flight, observing it at any given moment reveals a static state. However, in reality, motion is a continuous process over time, rather than a discrete instant, and there is no moment where the derivative of the arrow's displacement is zero, thus indicating that the arrow is indeed in motion.

The quantum Zeno effect borrows the concept from Zeno's paradox. During the evolution of a quantum system, if we measure the system, its wave function will collapse. When the measurement is continuous, the system will no longer evolve.

For example, there is a two-level system undergoing Rabi oscillations between state 1 and state 2. The probability of finding the system in state $|1\rangle$ at time t is

$$P_1(t) = \cos^2\left(\frac{\Omega_R t}{2}\right), \qquad (10)$$

and the probability of finding it in state $|2\rangle$ is

$$P_2(t) = \sin^2\left(\frac{\Omega_R t}{2}\right), \qquad (11)$$

where Ω_R is the Rabi frequency. If the time interval between measurements and the start of evolution is sufficiently short, $\Omega_R t \ll 1$, such that $P_1(t) \rightarrow 1$ and $P_2(t) \rightarrow 0$. Considering performing n projective measurements uniformly distributed over a total time t, the survival probability of the initial state of the system should be

$$P(t) = \cos^{2n}\left(\frac{\Omega_R t}{2n}\right). \qquad (12)$$

It can be seen that as $n \rightarrow \infty$, $P(t) \rightarrow 1$, which means when the measurement frequency is much higher than the oscillation frequency, the system will be frozen in state $|1\rangle$.

The measurement is performed by emitting a driving pulse with frequency ω_{13} at time t, which results in a projective measurement of the system. When the system collapses to state $|1\rangle$, it undergoes Rabi oscillations
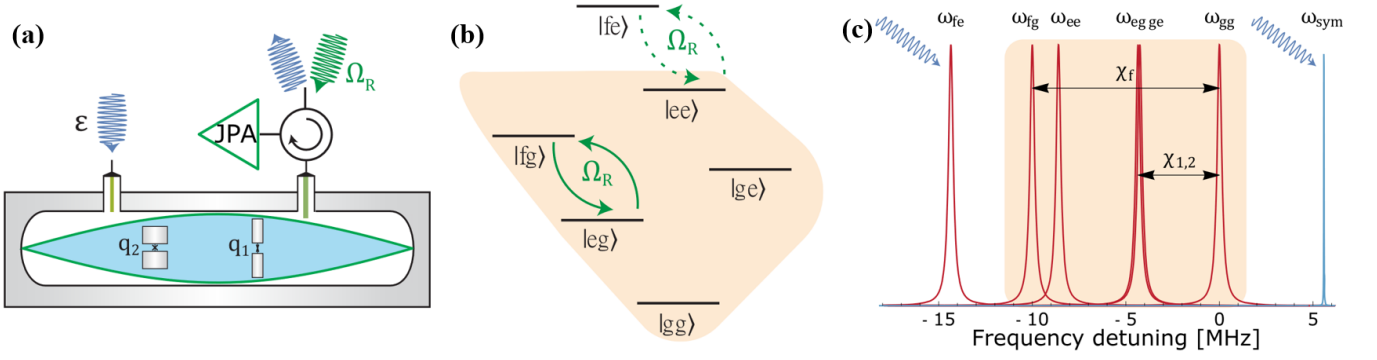
FIG. 2. Zeno Gate: (a) experimental Setup, (b) energy Level Structure, (c) frequency Detunings. Figure reproduced from [6].

between states $|1\rangle$ and $|3\rangle$, emitting a series of photons. After the measurement, the system returns to state $|1\rangle$ after one oscillation cycle. However, if the system collapses to state $|2\rangle$, no photons are generated, and the system remains in state$|2\rangle$ throughout the duration of the measurement.

The Zeno effect is relevant for engineered dissipation when the coupling to the environment is strong. Consider the case where, Instead of measurement our two-level system, we give an incoherent decay from $|2\rangle$ to $|1\rangle$, corresponding to the spontaneous emission of photons with a rate Γ and described by a Lindblad operator $L = \sqrt{\Gamma}\,|1\rangle\langle 2|$.

When the dissipation rate is much smaller than the Rabi frequency ($\Omega \gg \Gamma$), the system still undergoes Rabi oscillations. However, when the dissipation rate is much larger than the Rabi frequency($\Omega \ll \Gamma$), the dynamics conditioned by the absence of an dissipative event are described by a non-Hermitian effective Hamiltonian $H_{eff} = H - i\Gamma|2\rangle\langle 2|$. Therefor the state $|2\rangle$ acquires an imaginary phase, shifting its energy away from the real axis and introducing an effective detuning. The coupling between $|1\rangle$ and $|2\rangle$ becomes non-resonant, and the system is frozen in $|1\rangle$, achieving the same effect as multiple rapid measurements. Therefore, the quantum Zeno effect is not limited to systems that are explicitly measured, and dissipation can be interpreted as "measurements from the environment."

Therefore, we can utilize strong dissipation for coherent control of the system. For a three-level system with the energy level structure depicted in the figure, if a very strong dissipation is introduced to $|2\rangle$, the system will simply undergo Rabi oscillations between $|1\rangle$ and $|3\rangle$, never transitioning to $|2\rangle$. For this driven-dissipative system, the relevant subspace is formed by the states $|1\rangle$ and $|3\rangle$.

B. Zeno Gate

We can also achieve coherent control of a system using weak measurements. Consider a system where a quan-

tum three-level system and a qubit are dispersive coupled to a resonant cavity, but there is no interaction between q_1 and q_2. Fig.2(b) depicts the energy level structure of the system, and the right figure shows the dispersive spectrum. The cavity resonance frequencies for each state are well separated, and probing the cavity resonance frequency allows us to infer the state of the quantum three-level-qubit system. We achieve this by applying a driving pulse from one port and monitoring the output from another port. By applying a drive at ω_{fe}, we perform continuous measurement, equivalent to applying a projection P on the system.

The Hamiltonian under the Zeno effect is

$$
\begin{aligned}
H_{Zeno} &= PHP \\
&= i\hbar\frac{\Omega_R}{2}P(|e\rangle\langle f| - |f\rangle\langle e|) \otimes (|g\rangle\langle g| + |e\rangle\langle e|)P \\
&= i\hbar\frac{\Omega_R}{2}(|eg\rangle\langle fg| - |fg\rangle\langle eg|).
\end{aligned}
$$
(13)

where Rabi oscillations occur only between the eg and fg states.

Consider the time evolution operator

$$
U = \exp\left(-iH_{Zeno}t/\hbar\right)
$$
(14)

where $H_{Zeno} = i\hbar\frac{\Omega_R}{2}(|eg\rangle\langle fg| - |fg\rangle\langle eg|)$.

After evolving a period $t = 2\pi/\Omega_R$ $|eg\rangle$ will carry the phase of π, so a kind of phase gate can be realised, just as Fig.3 shows.

Fig.3(a) shows the evolutionary stages, demonstrating the modulation intervals in which they are located at different moments. And Fig.3(b) shows the evolution results, with the size of the squares representing the proportion of the distribution of the superposition states, and the colours representing the phases between the states. It can be seen that the eg state acquires a π phase after one cycle of evolution.
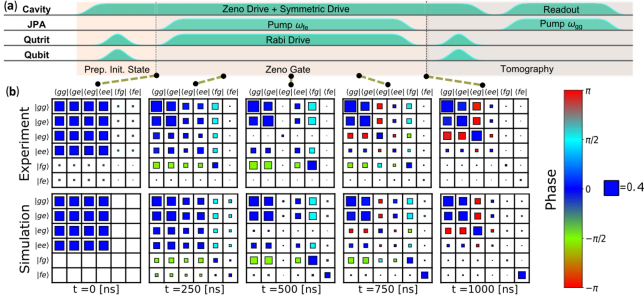
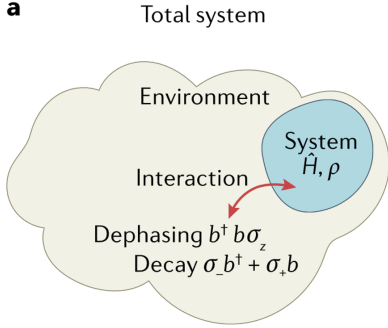FIG. 3. Phase gates (a) evolutionary stages (b) evolutionary results. Figure reproduced from [6].

FIG. 4. The dephasing and decay in quantum systems. Figure reproduced from [5].

IV. QUANTUM ERROR CORRECTION

A. Quantum Feedback

In the context of quantum computing, we aspire to achieve sufficiently long coherence times, which are often limited by noise from uncontrolled degrees of freedom. Quantum feedback is one of the methods to actively reduce noise and extend coherence times in these systems. Consequently, quantum feedback is also a crucial component of all proposals for fault-tolerant quantum computation.

One of the most significant applications of quantum measurement and feedback is quantum error correction. A typical approach to quantum error correction utilizes stabilizers or syndrome measurements, which refer to measurements that do not disturb the logical state but provide information that can be used to detect and correct errors. Quantum information is stored in a redundant manner, and syndrome measurements detect errors at a stage where they can still be corrected. Errors are corrected through gate operations that rotate the system back to the logical computational subspace, or syndrome measurements are recorded and an appropriate correction is applied at the end of the computation. When the interaction between a qubit and its environment leads to dissipation, the Lindblad operator is $L = \sqrt{\gamma}\sigma_-$ or $L = \sqrt{\gamma}a$.
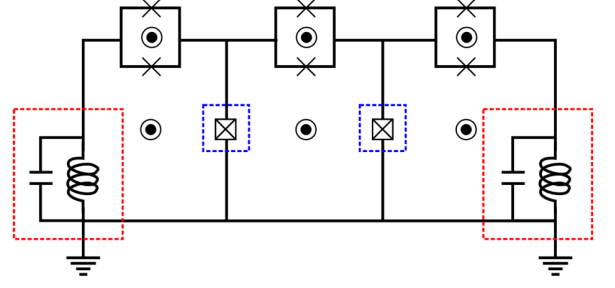

FIG. 5. The circuit of superconduction qubit for quantum error correction. Figure reproduced from [7].

B. Quantum Error Correction in Superconducting Circuit

Considering the circuit depicted in the Fig.5, which consists of two transmon qubits (with three energy levels, labeled as l and r), two LC resonators (labeled as Sl and Sr), and three SQUIDs. The Hamiltonian is

$$H = H_P + H_S + H_{PS},$$
$$H_P = -WX_lX_r + \frac{\delta}{2}(P_l^1 + P_r^1),$$
$$H_S = (W + \frac{\delta}{2})(a_{Sl}^\dagger a_{Sl} + a_{Sr}^\dagger a_{Sr}),$$
$$H_{PS} = \Omega(a_l^\dagger a_{Sl} + a_r^\dagger a_{Sr} + H.c.). \tag{15}$$

Here, $P_k^n = |n_k\rangle\langle n_k|$ $(n = 0, 1, 2 \ k = l, r), X_k = (a_k^\dagger a_k^\dagger + a_k a_k)/2.$

Labeling $|L_0\rangle$ and choose to act as our logical state manifold:

$$|L_0\rangle = \frac{|0_l\rangle + |2_l\rangle}{\sqrt{2}} \otimes \frac{|0_r\rangle + |2_r\rangle}{\sqrt{2}} \otimes |0_{Sl}0_{Sr}\rangle. \tag{16}$$

First, tackling photon loss errors, a white noise error source which to a good approximation occurs at rates independent of many-body energetics. Without loss of generality, we consider a single-photon loss in the left qubit, which sends

$$a_l|L_0\rangle = |1_l\rangle \otimes \frac{|0_r\rangle + |2_r\rangle}{\sqrt{2}} \otimes |0_{Sl}0_{Sr}\rangle. \tag{17}$$

However, these states are not eigenstates of H, In the limit $W \gg \Omega$, the full single-photon excited states are

$$|E_{0\pm}\rangle = \frac{1}{\sqrt{2}}\left[|1_l\rangle \otimes \frac{|0_r\rangle + |2_r\rangle}{\sqrt{2}} \otimes |0_{Sl}0_{Sr}\rangle \right.$$
$$\left. \pm \frac{|0_l\rangle + |2_l\rangle}{\sqrt{2}} \otimes \frac{|0_r\rangle + |2_r\rangle}{\sqrt{2}} \otimes |1_{Sl}0_{Sr}\rangle\right]. \tag{18}$$

Therefore,

$$a_l|L_0\rangle = \frac{|E_{0+}\rangle + |E_{0-}\rangle}{\sqrt{2}}. \tag{19}$$

In this case, the state is exactly a superposition of single-photon excited states. Error correction can be achieved by rapidly dissipating the photon in the resonator.
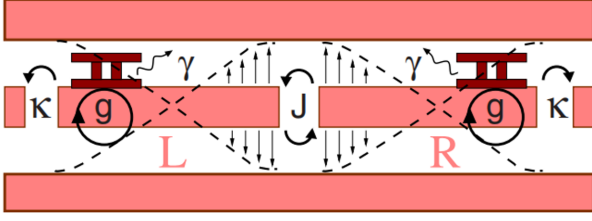
FIG. 6. Schematic of superconducting quantum circuit coupling. Figure reproduced from [8].

V. QUANTUM SIMULATION

Dissipative systems are widely used in quantum simulation, allowing for the observation of rich phase diagrams and the realization of some exotic stable phases.

A. Two-Body Jaynes-Cummings Model

For example, dissipative Phase Transition in the Two-Body Jaynes-Cummings Model is shown in Fig.6. For the traditional interaction between light and a two-level atom, the $\hat{H}$ in RWA is

$$\hat{H}^{JC} = \nu_c \hat{a}^\dagger \hat{a} + \nu_a \hat{\sigma}^+ \hat{\sigma}^- + g\left(\hat{\sigma}^+ \hat{a} + \hat{\sigma}^- \hat{a}^\dagger\right). \quad (20)$$

Extending to a two-body system with a cavity field coupled to each side separately

$$\hat{H}^{dimer} = \sum_{s=L/R} \hat{H}^{JC}_s - J\left(\hat{a}^\dagger_L \hat{a}_R + \hat{a}^\dagger_R \hat{a}_L\right), \quad (21)$$

where J represents the hopping of phonons between the two sides, and the master equation is

$$\frac{\partial \hat{\rho}}{\partial t} = i\left[\hat{\rho}, \hat{H}^{dimer}\right] + \sum_{i=L,R}\left(\frac{\kappa}{2}\mathcal{L}\left[\hat{a}_i\right] + \frac{\gamma}{2}\mathcal{L}\left[\hat{\sigma}_i^-\right]\right), \quad (22)$$

where $\mathcal{L}[\hat{O}] = 2\hat{O}\hat{\rho}\hat{O}^\dagger - \hat{\rho}\hat{O}^\dagger\hat{O} - \hat{O}^\dagger\hat{O}\hat{\rho}$ is a Liouvillian superoperator characterizing the dissipation of the system.

To prepare coherent states for measurement, we consider studying

$$\begin{aligned} \hat{I} &= \frac{\hat{a} + \hat{a}^\dagger}{2}, \\ \hat{Q} &= i\frac{\hat{a}^\dagger - \hat{a}}{2}, \end{aligned} \quad (23)$$

Homodyne Signal is

$$\xi = \left\langle \hat{I} \right\rangle^2 + \left\langle \hat{Q} \right\rangle^2, \quad (24)$$

and the number of photons should be $\left\langle \hat{I}^2 + \hat{Q}^2 \right\rangle$.

The Fig.7(a)(b) depicts the experimental circuit, which consists of two transmon qubits, each coupled to
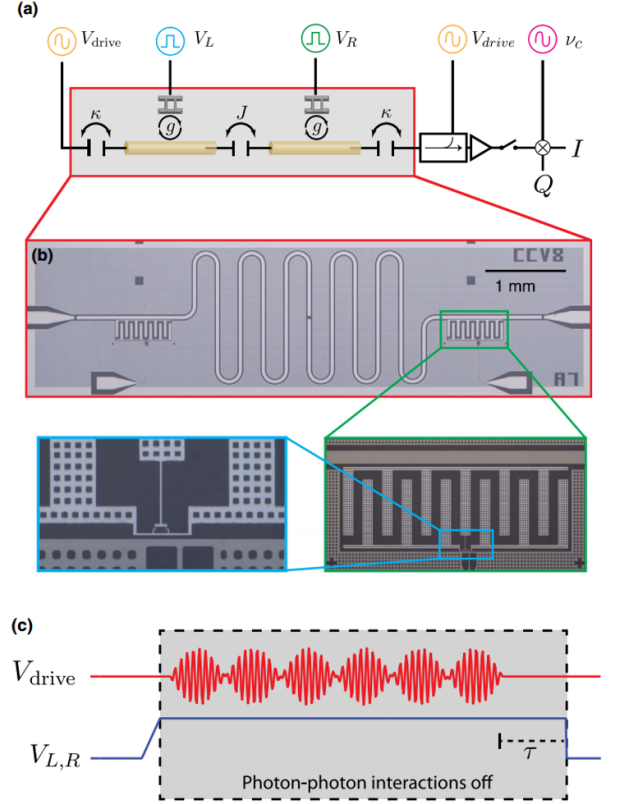

FIG. 7. Experimental setup and signal pulse waveform. Figure reproduced from [9].

a resonant cavity. The hopping is achieved by a capacitor placed in the middle of the resonant cavities. The Fig.7(c) shows the driving signal. At the beginning of the experiment, the cavities are first excited by the driving signal while the control qubits are both in their ground states. Once the excitation reaches the target cavity population, the qubit driving is shut off at an arbitrary time and the interaction is turned on, thereby obtaining different non-steady states. This moment is marked as the start of the measurement.

During the experiment, a phase transition was observed. When the photon number is less than a certain threshold, the system transitions from non-local oscillations and linear exponential decay to nonlinear super-exponential decay. After the signal decays to zero, it stabilizes to a local state.

The experimental results are shown in Fig.8. Fig.8(a) measures the state with and without photon interaction. The red line represents the case without interaction, where the signal exhibits continuous exponential decay. The blue line is the measurement with interaction turned on, and it can be seen that after a period of time, it transitions to super-exponential decay. Fig.8(b) shows measurements with different initial populations, demonstrating that a phase transition occurs at a threshold value for all cases. Fig.8(c) adds measurements of photon numbers, revealing that while there are still photons
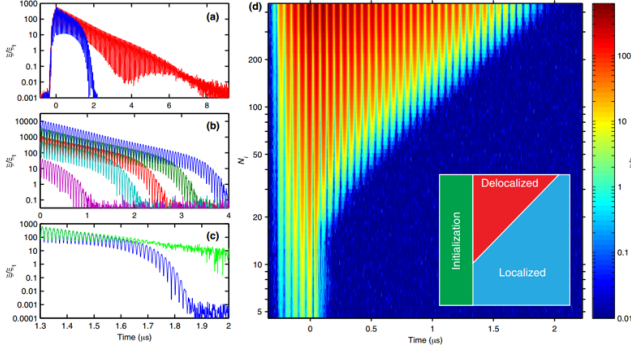
FIG. 8. Experimental measurement results for Two-Body Jaynes-Cummings model. Figure reproduced from [9].
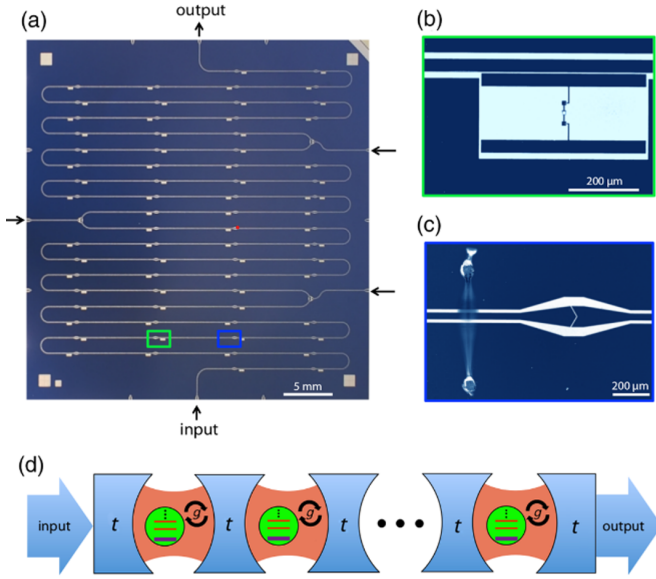

FIG. 9. 1D cQED lattice (a) experimental setup (b) (c) detail view (d) equivalent model. Figure reproduced from [10].

present in the local state, the oscillation phenomenon has disappeared. The phase diagram Fig.8(d) shows two distinct phases: the local state and the non-local state.

B. Dissipative Phase Transitions In a 1D cQED Lattice

We can attempt to generalize the model to a multi-body system by introducing dissipation to each component. This generalization can be applied to a multi-body model, for instance, where 72 transmon qubits are individually coupled to resonators and then interconnected. Transmission intensity can be measured from the first node as the input and the final node as the output.

Using one-dimensional circuit quantum electrodynamics (cQED), a Bose-Hubbard-like model can be constructed, which is coupled to cavities. The corresponding
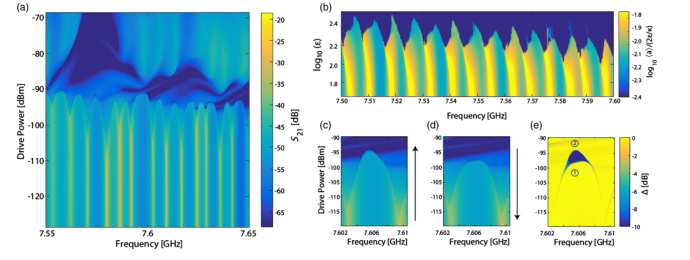

FIG. 10. 1D cQED lattice experimental and simulation results. Figure reproduced from [10].

Hamiltonian is

$$H = \sum_j \left(H_j^r + H_j^q + H_j^{rq} \right) + \sum_{\langle j,j' \rangle} H_{j,j'}^{hop} + H^d. \quad (25)$$

where resonator energy $H_j^r = \hbar\omega_c a_j^\dagger a_j$. Transmon qubit energy $H_j^q = \hbar\Omega_j b_j^\dagger b_j + \frac{1}{2} U b_j^\dagger b_j^\dagger b_j b_j$, means the latter having the Hubbard interactions. Weak interactions between resonator and quantum bits using the rotating wave approximation $H_j^{rq} = \hbar g_j (a_j b_j^\dagger + H.c.)$. The hopping term for the nearest-neighbour resonator phonon $H_{j,j'}^{hop} = \hbar t (a_j a_{j'}^\dagger + H.c.)$. And the first node microwave drive term $H^d = \hbar\epsilon(t) a_1 e^{i\omega_d t} + H.c..$

The transmission spectrum was experimentally observed with respect to the driving intensity and frequency. It is found that at higher driving intensities, the resonance peaks and local minima at lower times are no longer present, but a region of strong suppression is present, as shown in Fig.10(a). It can be seen that two phases clearly appear, and a hysteresis phenomenon is also observed, as shown in Figs.10(c)(d). An increase in drive strength stays in the resonant localised phase for an additional period, while a decrease in drive strength has the same effect.

The transmission intensity should be related to the average value of the annihilation operator, and the master equation is

$$\frac{\partial\rho}{\partial t} = \frac{i}{\hbar}[\rho, H] + \sum_j \left(\frac{\kappa}{2}\mathcal{L}[a_j] + \frac{\Gamma}{2}\mathcal{L}[b_j] \right) \quad (26)$$

Utilizing the mean-field approximation, making $\alpha_j = \langle a_j \rangle$ and $\beta_j = \langle b_j \rangle$, we obtain the dynamical evolution that satisfies[11]

$$i\dot{\alpha}_j = \left(\omega_c - \omega_p - i\frac{\kappa}{2} \right) \alpha_j + g_j\beta_j + t(\alpha_{j-1} + \alpha_{j+1}) + \epsilon\delta_{j,1}$$

$$i\dot{\beta}_j = \left(\Omega_j - \omega_p - i\frac{\Gamma}{2} \right) \beta_j + \frac{U}{\hbar}|\beta_j|^2\beta_j + g_j\alpha_j$$

$$(27)$$

Fig.10(b) plots the average value of the annihilation operator for the last cavity, and it can be seen that it exhibits qualitative consistency with the experimental results.
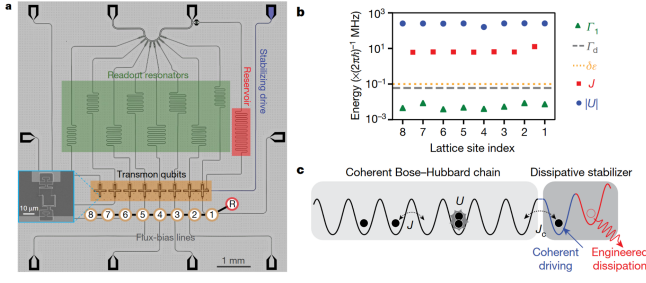
FIG. 11. 8-node superconducting quantum circuit (a) experimental setup (b) parameter measurements (c) equivalent model. Figure reproduced from [12].
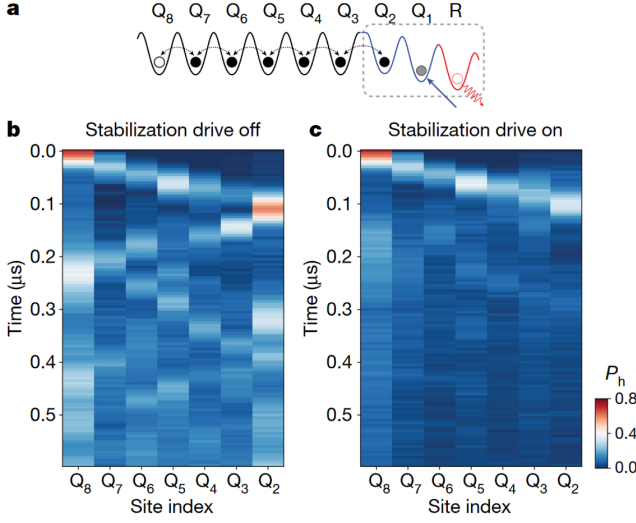

FIG. 12. Quantum walk (a) Equivalent node (b) Quantum walk without dissipative drive (c) Results with dissipative drive on. Figure reproduced from [12].

C. Dissipation-stabilised Photonic Mott Insulators

Considering the Bose cold atom system, in which the two most classical phases are the superfluid phase and the Mott insulator phase. These phases can be analyzed using the mean-field approximation. Here, we have constructed an analogous Bose-Hubbard chain using superconducting quantum circuits, which consists of 8 transmon qubits, a coherent drive on the right side, and dissipation, just as Fig.11(a) shows. The experimental parameters for each node are shown in Fig.11(b).

Fig.11(c) shows the equivalent model with the Hamil-

tonian

$$H_{BH} = -\sum_{\langle i,j\rangle} J_{ij} a_i^\dagger a_j + \frac{U}{2}\sum_i n_i(n_i-1) + \sum_i \epsilon_i n_i \quad (28)$$

The two rightmost nodes serve as dissipation stabilizers, which can stabilize the Mott insulator phase. The physical process involves the injection of two photons into the middle node using a coherent drive when both nodes are in a hole-occupied state. These photons undergo elastic collisions and are distributed to the two side nodes. However, due to the rapid dissipation of photons in the rightmost node, the state remains highly stable, ensuring that the left node does not experience hole occupation.

In the experiment, we first control the leftmost node to be in a hole-occupied state. It can be observed that this state propagates through the Bose-Hubbard chain. When the dissipation stabilizer is turned off, the hole state continues to propagate in the chain, exhibiting a quantum walk, as shown in the Fig.12(b). However, when we turn on the dissipation stabilizer, the hole state is immediately replenished upon reaching the rightmost node, ensuring that there are no unoccupied nodes in the system. This is analogous to the Mott insulator phase in the Bose cold atom system, as depicted in the Fig.12(c).

VI. SUMMARY

First, we introduced the master equation, a mathematical theoretical method used to describe dissipative systems. Then, we discussed the Zeno effect, which utilizes rapid measurements to maintain the state of a system and can be used to construct logic gates. Next, we delved into dissipation in quantum error correction, where dissipation can be harnessed to correct the state of a system. Finally, we presented quantum simulation, highlighting that the addition of dissipation can introduce a wealth of phases to a system and enable the stabilization of these phases.

Similarly, there is considerable progress in quantum dynamical systems[13]. These differ from their classical counterparts not only owing to the structure of the underlying microscopic equations, but also owing to the importance of quantum entanglement. Dissipative systems hold significant applications and research value in physics, and there are still many open questions to be explored.

[1] D. Manzano, A short introduction to the lindblad master equation, Aip Advances **10** (2020).

[2] H.-P. Breuer and F. Petruccione, *The theory of open quantum systems* (OUP Oxford, 2002).

[3] 郭光灿, 量子光学 (科学出版社, 北京, 2022).

[4] 张智明, 量子光学 (科学出版社, 北京, 2015).

[5] P. M. Harrington, E. J. Mueller, and K. W. Murch, Engineered dissipation for quantum information science, Nature Reviews Physics **4**, 660 (2022).

[6] K. Geerlings, Z. Leghtas, I. M. Pop, S. Shankar, L. Frunzio, R. J. Schoelkopf, M. Mirrahimi, and M. H. Devoret, Demonstrating a driven reset protocol for a su-

perconducting qubit, Physical review letters **110**, 120501 (2013).

[7] E. Kapit, Hardware-efficient and fully autonomous quantum error correction in superconducting circuits, Physical review letters **116**, 150501 (2016).

[8] S. Schmidt, D. Gerace, A. Houck, G. Blatter, and H. E. Türeci, Nonequilibrium delocalization-localization transition of photons in circuit quantum electrodynamics, Physical Review B **82**, 100507 (2010).

[9] J. Raftery, D. Sadri, S. Schmidt, H. E. Türeci, and A. A. Houck, Observation of a dissipation-induced classical to quantum transition, Physical Review X **4**, 031043 (2014).

[10] M. Fitzpatrick, N. M. Sundaresan, A. C. Li, J. Koch, and A. A. Houck, Observation of a dissipative phase transition in a one-dimensional circuit qed lattice, Physical Review X **7**, 011016 (2017).

[11] U. Naether, F. Quijandria, J. J. García-Ripoll, and D. Zueco, Stationary discrete solitons in a driven dissipative bose-hubbard chain, Physical Review A **91**, 033823 (2015).

[12] R. Ma, B. Saxberg, C. Owens, N. Leung, Y. Lu, J. Simon, and D. I. Schuster, A dissipatively stabilized mott insulator of photons, Nature **566**, 51 (2019).

[13] A. Polkovnikov, K. Sengupta, A. Silva, and M. Vengalattore, Colloquium: Nonequilibrium dynamics of closed interacting quantum systems, Reviews of Modern Physics **83**, 863 (2011).